ADVANCED ENERGY MATERIALS
www.advenergymat.de

Layer-by-Layer Processed Pseudo-Bilayer Heterojunctions Advance the Performance of Organic Solar Cells

Donghui Li, Austin M. Kay, Drew B. Riley, Oskar J. Sandberg, Ardalan Armin, and Paul Meredith**

Recent progress in organic (semiconductor) solar cells (OSCs) has led to power conversion efficiencies (PCEs) reaching 20%, with predictions that 25% may be possible. Additional to PCE improvements, significant efforts have been made to address the engineering challenges that have traditionally limited OSCs small area devices often with poor temporal stability. Layer-by-layer (LbL) processing of active layers has emerged as a promising approach to tackle these challenges, with numerous state-of-the-art OSCs processed using LbL reported. In this Perspective, recent developments are developed in enhancing OSC efficiency and stability, with a particular focus on the working mechanisms of pseudo-bilayer heterojunctions (P-BHJ) and the practical aspects of fabricating high-performance devices using LbL techniques. By providing insights into LbL processing and the resultant film morphology, it is hoped to contribute to the ongoing efforts to improve OSC efficiency, stability, and scalability and to explore their potential for broader applications such as for example for indoor light harvesting or agrivoltaics.

1. Introduction

Organic solar cells (OSCs) have attracted significant attention in the context of clean energy generation due to their potential advantages, mainly related to ease of processing, potential for low cost, low embodied manufacturing, and tailorable optical properties.[1–3] Through extensive research efforts in molecular design, fundamental operating principles, and device engineering, single junction OSCs have now reached power conversion efficiencies (PCE) of 20%,[4–6] with the potential to reach 25%.[7] Despite this notable improvement, commercialization of OSCs has remained a big challenge due mainly to stability and scalability issues limiting OSCs to small area cells with short lifespan or, modules with thin-strip serial connected architectures.[8]

The typical structure of an OSC is an anode, a cathode, charge transport layers, and an active layer sandwiched between them.[9] The structure and morphology of the active layer greatly affects photon absorption, exciton dissociation, charge transport, and PCE.[10] To overcome the limitations of the planar heterojunction (PHJ) active layer configuration formed by sequential deposition of (p-type) donor and (n-type) acceptor materials,[11] the bulk heterojunction (BHJ) strategy was introduced.[12] BHJs have many donor (D)/acceptor (A) nanoscale interfaces within the active layer due to nanoscopic phase separation of the donor and acceptor blend, facilitating the separation of electron-hole pairs (excitons) via the formation of interfacial charge-transfer (CT) states. This enables efficient charge carrier generation,[10] which is essential for generating photocurrent and photovoltage. The BHJ active layer is formed by blending electron donor and acceptor in a solution and depositing in a single step. Ultimately, the use of BHJs has enabled the realization of numerous high-performance OSCs, with record PCEs now reaching 20.8%.[13]

The donor and acceptor molecules in state-of-art OSCs possess multi-scale conjugated structures,[14,15] resulting in complex intermolecular interactions, self-organization during processing, and spontaneous phase separation in the solid state when blended together.[16,17] Moreover, the morphological state of the system may be kinetically metastable, rather than being thermodynamically stable.[18] Therefore, after prolonged light exposure or thermal aging, significant morphological degradation may occur,[19,20] including donor/acceptor domain decomposition and interface shrinkage as well as excessive phase separation,[21] which lead to severe degradation of charge transport and a shortened device lifetime.[22] Additionally, vertical stratification within the film is influenced by surface and interface effects;[23] as such achieving an optimal phase distribution requires a significant driving force from the structural features and miscibility of the materials involved.

D. Li, A. M. Kay, D. B. Riley, A. Armin, P. Meredith
Sustainable Advanced Materials (Sêr-SAM)
Centre for Integrative Semiconductor Materials (CISM)
Department of Physics
Swansea University Bay Campus
Swansea SA1 8EN, UK
E-mail: ardalan.armin@swansea.ac.uk; paul.meredith@swansea.ac.uk
O. J. Sandberg
Faculty of Science and Engineering
Åbo Akademi University
Turku 20500, Finland

The ORCID identification number(s) for the author(s) of this article can be found under https://doi.org/10.1002/aenm.202500816

DOI: 10.1002/aenm.202500816

To go beyond blended BHJ OSCs, the layer-by-layer (LbL) processed pseudo-bilayer heterojunction (P-BHJ) has been developed as an alternative.[24,25] The LbL processing method involves depositing donor and acceptor materials in sequence, offering significant advantages in film preparation[26] and morphology fine-tuning compared to BHJ processing. This allows for individual pre-treatment of both the donor and acceptor molecules before they are mixed,[27] providing greater flexibility for controlling pre-aggregation of the materials, which is beneficial for achieving an ideal morphology and phase separation in the resulting active layer.[26,28] Furthermore, a gradual interface inducing a non-continuous phase structure can form in a P-BHJ, which can result in radically different exciton and charge dynamics compared to the BHJ case, possibly including reductions in bimolecular recombination leading to improved fill-factors.[27–29] Additionally, owing to the superior p-i-n vertical phase distribution, LbL processed active layers are expected to exhibit a narrower density of states (DOS).[32] As a result, LbL processing has elevated the PCE of OSCs to values comparable to or even surpassing those achieved with BHJ approaches.[33]

Research into P-BHJ OSCs began alongside research on BHJ OSCs, but due to large intermixing between donor and acceptor molecules and limited exciton diffusion coefficients, their performance generally lagged behind BHJs made from the same materials. Moreover, P-BHJ active layers require additional fabrication steps and fine control of each layer (e.g., thickness), which increases complexity impacting reproductivity. In addition, LbL processing may not always be effectively applied to inverted devices based on polymer:small molecule systems, in which the small molecules are deposited first with subsequent depositions destroying the small molecule film.

More recently, however, the introduction of new donor and acceptor materials has led to a renaissance in LBL processing where P-BHJ devices are now competitive with their BHJ counterparts. In this Perspective, we systematically analyze the film processing, morphological characteristics, exciton diffusion, and charge transport dynamics in P-BHJ OSCs, and introduce the potential advantages of P-BHJs to upscaling and stability required for more viable uptake of OSC technology. Advancing a comprehensive understanding of the relationship between processing technique and film structure is crucial for optimizing device performance, which could help fine-tune P-BHJ active layer and is expected to guide directions for future development of P-BHJ OSCs, particularly for application targets such as building-integrated photovoltaics, agrivoltaics, and indoor photovoltaics.

2. Active Layer Fabrication

Molecular packing, aggregated states, and film processing during active layer preparation are vital for achieving high-performance OSCs. First, we will examine the contribution of organic semiconducting materials to the performance of the active layer.[34–36] Then, we will show the importance of the processing method in controlling film morphology and the resulting properties of the active layer.

2.1. Organic Semiconducting Materials

OSCs are typically made from a blend of two organic semiconductors known as the donor and the acceptor, often denoted as D:A. Common blends include polymer:fullerene, polymer:small molecule, polymer:polymer, small molecule:small molecule, and multi-component blends.[37] The intrinsic properties of the chosen materials and the type of heterojunction formed will greatly affect the electron and hole transport properties in the device, thereby affecting the open circuit voltage (V_{OC}), short-circuit current density (J_{SC}), and fill-factor (FF). For acceptor materials, fullerene derivatives with "ball-like" molecular structures were commonly chosen in early studies, with OSCs based on PC_{71} BM (see Supporting Information) achieving PCEs of up to 11.7%.[38] Concurrent efforts to develop non-fullerene acceptors (NFAs) such as the PDI series of materials (e.g., Phenyl-PDI) were less successful.[39] These 2D planar molecules are likely to self-assemble into large crystalline structures, leading to excessive phase separation and a reduced donor/acceptor interface in the film, resulting in non-ideal device performance.[40,41]

On the other hand, the development of A-D-A and A-D-A-D-A type NFAs (e.g., ITIC and Y6) with tailored absorption spectra and energy levels led to a step-like increase in the PCE.[14,15] Generally, the Y-series acceptors (including Y6 and L8-BO) exhibit a broad absorption spectrum extending into the near-infrared region (i.e possess narrow optical gaps), which increases the absorption under solar conditions leading to larger J_{sc}. Additionally, the Y-series acceptors exhibit a preference for face-on orientation and close π–π stacking, expected to be beneficial for charge transport. As seen in **Figure 1**, these molecules have various stacking and aggregation patterns, enabling them to form multi-dimension intermolecular networks; the Y-series (L8-BO and Y6) show a honeycomb network,[42–44] thereby facilitating efficient charge transport.[45] It is also thought that Y-series acceptors in their neat phase can generate long-lived free charges with an ambipolar mobility environment,[46] which can be readily extracted using energetically tailored transport layers. Notably, the exciton diffusion length (L_D) of the Y-series acceptors is usually several fold that of the earlier materials (i.e., fullerene and IT-series acceptors),[47,48] enabling efficient exciton diffusion to a donor/acceptor interface; this promotes the development of high-performance P-BHJ OSCs, and makes Y-series acceptors very suitable for realizing high-performance LbL processed OSCs.

2.2. LbL Processing

While significant attention is always directed to the development of state-of-the-art materials, film processing is equally crucial in the fabrication of high-quality thin films from solution.[49] P-BHJ film formation is driven by the swelling-penetration of materials and solvents and has the potential to create stable morphologies optimized for OSCs. **Figure 2**a,b illustrate the differences between blended and LBL processing. As previously mentioned, blended processing consists of creating a solution of donor and acceptor materials and depositing onto the substrate in one step. In contrast, LbL processing consists of depositing a solution of the donor material on the substrate followed by a solution of the acceptor material. It is understood that the donor

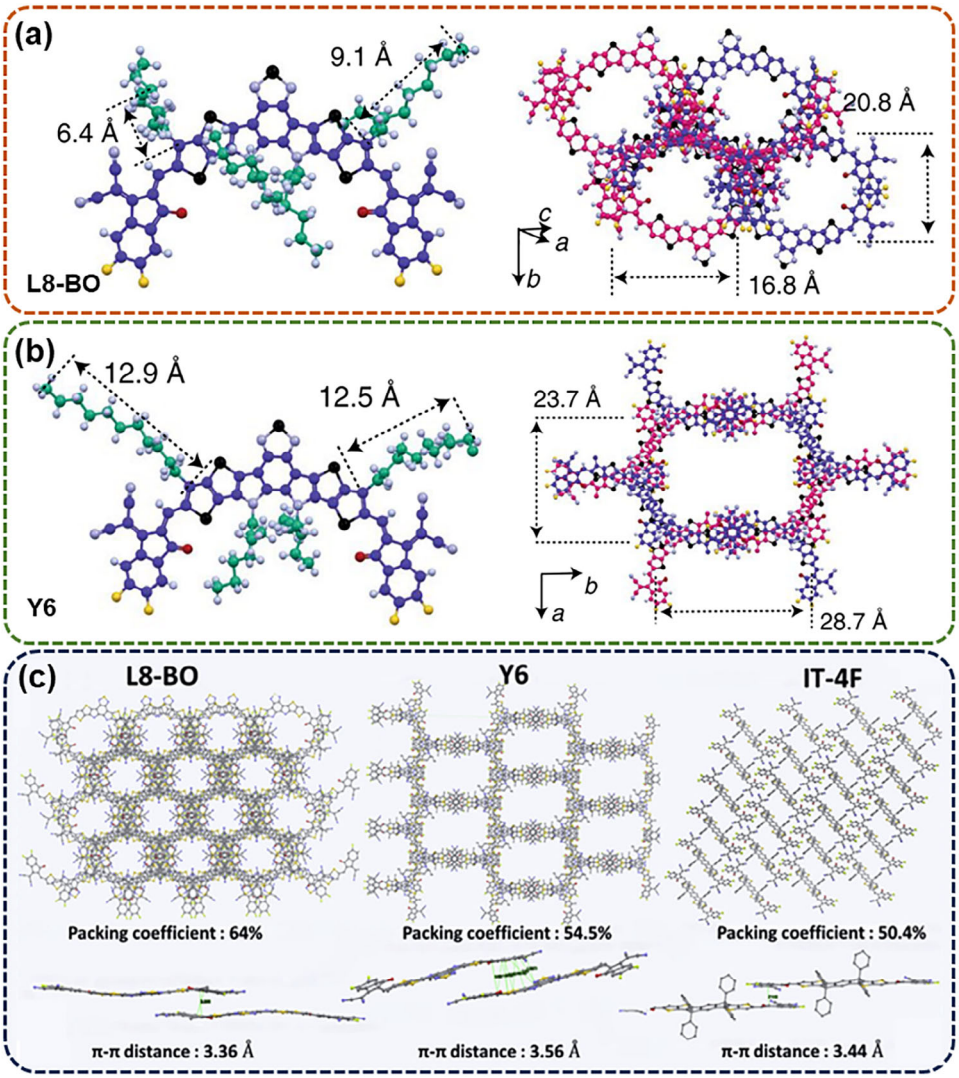

Figure 1. Single-crystal structures and molecular packing properties of NFAs: The main view of a molecular conformation and packing sketch of a) L8-BO and b) Y6, the dashed lines represent the side-chain self-assembly distance of NFAs. (Reproduced with permission.[42] Copyright 2021, Springer Nature). c) Illustrated molecular packing properties of L8-BO, Y6, and IT-4F. (Reproduced with permission.[44] Copyright 2022, Elsevier).

material forms a scaffold that the acceptor material gradually penetrates through the swelling effect of the acceptor solvent (see Figure 2c).[50] This process will lead to dynamic molecular interactions, co-driving phase separation in the resulting film with solvents evaporation,[51] which is also called the swelling-intercalation-phase-separation (SIPS) effect.[52,53] Thus, the properties of the solvent, such as polarity and boiling point, have a large effect on the SIPS process. By controlling the processing conditions, phase distribution and film morphology can be varied. Russell et al.[54] deposited PC_{71} BM dissolved in various solvents including toluene, *ortho*-xylene (*o*-XY), chlorobenzene (CB), and 1,2-dichlorobenzene (DCB) onto pDPP films, then found that toluene and *o*-XY exhibited limited swelling, resulting in PC_{71} BM being confined to the shallow surface layer of the pDPP film. However, CB and DCB exhibit effective penetration and contact between PC_{71} BM and pDPP because of the better solvent swelling.

Solvents can also induce a solution-incubated pre-aggregation (SIPA) effect on materials,[55] which is significant for regulating the crystallinity and molecular aggregates of both donors and acceptors. Weakly-crystalline organic semiconductors predominantly show an amorphous state after film formation with discontinuous carrier transport channels and low mobility. The SIPA strategy can adjust the solvent-solute interaction via solution aging or the addition of an anti-solvent, inducing organic semiconductors to form pre-aggregates that act as nucleating agents to increase crystallinity, thereby forming a more desirable phase-separated structure. Additives can further enhance this effect, offering a versatile means of manipulating the molecular structure and materials properties in the active layer.[56,57] The additives are not necessarily a different material to the host donor and acceptor, Wang et al. grew polymer polycrystals through a vapor diffusion method and employed as an additive to effectively regulate the crystallinity and molecular aggregates of both donors and

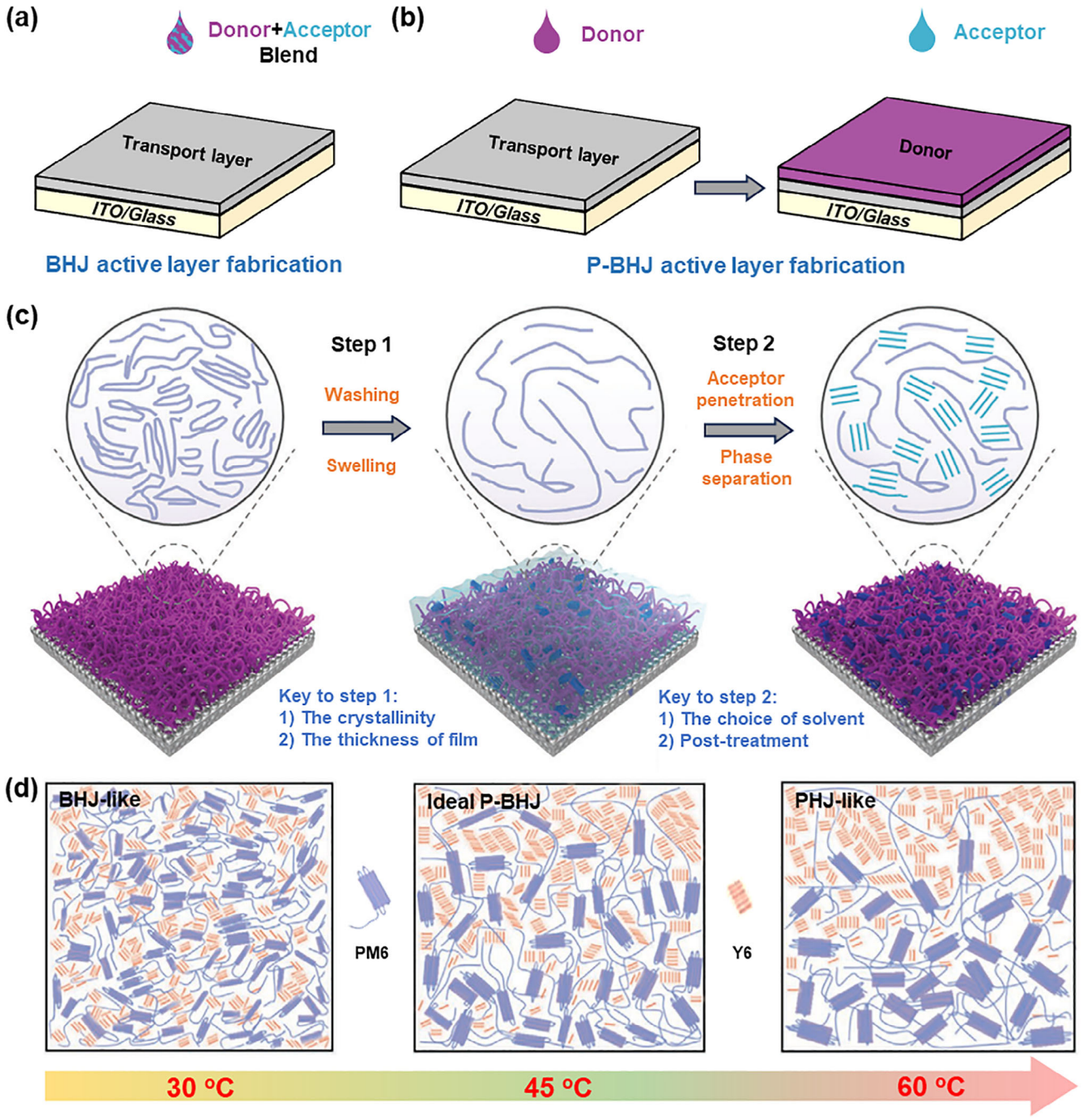

Figure 2. Diagram of fabrication procedures for a) BHJ and b) P-BHJ active layers. c) Schematic illustration of the swelling-penetration process: the processing solvent first swells the pre-deposited donor polymer matrix, and then the acceptors penetrate the gel-like polymer to form the active layer. (Reproduced with permission.[50] Copyright 2024, Wiley-VCH). d) The evolution of morphological characteristics and fundamental processes as a function of baseplate temperature. (Reproduced with permission.[65] Copyright 2021, Wiley-VCH).

acceptors.[56] The nanoscale polymer polycrystals were found to trigger molecular organization at a lower solid content, therefore prolonging the whole crystallization time to increase structural order.

Wang et al.[58] developed an innovative approach to regulate the molecular order of polymer donors, where they designed and added electronegative INMB-F into a range of electropositive polymer donors, including PM6, D18-Cl, and PTB7-Th. The resultant electrostatic force between INMB-F and the polymer donors leads to enhanced structural order and charge transport, improving both device efficiency and stability. They continued by adopting 1-fluoronaphthalene (FN) as the additive into the acceptor layer L8-BO, finding that FN acts as a molecular bridge to enhance conjugation between L8-BO molecules, resulting in

the formation of L8-BO fibrils.[59] Deposition of the fibrils on the donor D18 (processed by CF solvent), resulted in 19% efficiency OSCs with a pronounced fibrillar network active layer, which is an improvement over the 16% efficiencies of the traditional BHJ and P-BHJ devices without additives. These results demonstrate the advantages of fibrillar components in the photoactive layer in enhancing the short-circuit current and fill factor. Additionally, it also illustrates how P-BHJ film processing provides a window for pre-optimizing the crystallinity of materials[60,61] by treating donor films before acceptor deposition and active layer formation. Moreover, the conjugated units in the molecular structure may guide acceptor molecules to further self-assemble within the donor scaffold, then induce molecular arrangement and crystallization, all of which would affect the active layer significantly.

Temperature control is a critical factor in P-BHJ film processing, showing pronounced effects on the SIPS aspect and final film morphology.[62–64] As depicted in Figure 2d, varying the temperature of the substrate during processing leads to differing phase separation and morphological evolution in LBL processed films. At lower temperatures a BHJ-like morphology is formed where the two molecules are fully intermixed, creating small domains of each molecule. As the temperature gradually increases, phase separation and PHJ-like morphology appear. Excessive temperatures (>60 °C) will lead to a short drying time of solvent (which is CF in this case) and insufficient permeation, resulting in an inferior donor/acceptor interface area and poor exciton separation.[65] Optimal temperatures, typically around 45 °C, yield films with an optical vertical phase distribution characterized by a pronounced p-i-n effect and enhanced domain purity, conducive for efficient charge transport and carrier extraction. Vacuum post-treatment has been shown to optimize the migration of molecules within films leading to a well-defined vertical phase distribution.[66] This allows for mutual diffusion between components in films from solution to solid-state, encouraging nanoscale phase-separated interpenetrating networks in the active layer.[67] Additionally, similar conjugated units between the molecular structures in both donor and acceptor may facilitate the assembly and rearrangement of molecules during the solution penetration in LbL processing, which may alter the molecular packing and crystallization,[68] thereby affecting the morphology within the active layer. This vertical phase separation can create active layers that are more thermodynamically stable than BHJs while maintaining the charge collection capabilities.

2.3. Morphology in P-BHJ Active Layers

Morphology control in the active layer has significant impacts on charge transport and recombination and has been proven to be the key to regulating the performance of OSCs. LbL processing can accommodate an extended parameter space for constructing a more ideal morphology than the traditional BHJ method, and achieving the p-i-n structure and a gradual interface.[69] Jiang et al.,[70] compared the morphological behavior in traditional BHJ and LbL processed P-BHJ active layers based on PM6:N3, through grazing-incidence wide-angle X-ray scattering (GIWAXS) characterization (see **Figure** 3a,b). They found favorable molecular ordering occurring in P-BHJ films along with enhanced phase separation and crystallinity of PM6 and N3. Li et al.[59] revealed intriguing insights into the role of conjugated D18 and FN molecules in inducing the formation of fibril aggregates in the NFA L8-BO. As shown in Figure 3d,e, while BHJ films have a random dispersion of D18 and L8-BO, LbL films exhibited a distinct L8-BO-rich fibrillar top layer, this p-i-n like vertical distribution has the advantage of efficient charge collection as the morphology minimizes recombination while maintaining efficient charge separation. Similar findings also appeared in films based on PM6:PY-V-γ; as seen in Figure 3f, the P-BHJ film shows more fibrillar feature compared BHJ film from the atomic force microscopy (AFM) images.[71] Grazing-incidence small-angle X-ray scattering (GISAXS) analysis demonstrated a slightly enlarged phase separation in P-BHJ film compared to BHJ film (see Figure 3c),[55,59] suggesting the potential of LbL processing in constructing optimal interfaces and morphologies. Furthermore, this type of fibrillar morphology is thought to act as a 3D network for enabling charge transport.

As opposed to the traditional BHJ approach, the p-i-n like morphology in P-BHJ active layers offers a route to optimizing the performance of OSCs. Results from photoluminescence (PL) spectroscopy (shown in Figure 3g,h) indicate a directional dependence where donor signals (600–800 nm) are observable from the back side but are absent from the front side in LbL processed P-BHJ films; in contrast, PL is dominated by acceptors (800–1100 nm) from both sides in BHJ films.[70] This study demonstrates the differences in vertical structure between traditional BHJ and P-BHJ films. Figure 3i further reveals p-i-n like vertical phase distribution profiles within LbL processed active layers with deep etching X-ray photoelectron spectroscopy (XPS) techniques.[72] The time-of-flight secondary ion mass spectrometry (ToF-SIMS) measurement by tracking Se^{2-} in the T9SBN-F molecule demonstrates that acceptor content is enriched near the cathode and the donor content is enriched near the anode, reflecting a gradient composition distribution occurring in P-BHJ films.[69,73,74] Whereas, in the BHJ the proportion of Se is consistent throughout the heterojunction. These investigations not only shed light on the features of gradual interface and optical vertical distribution in LbL processing but also demonstrate that p-i-n like structure has the potential to enhance charge separation, as stated earlier.

Through an investigation into the LbL fabrication approach using solvents with varying boiling-points, it was found that the interpenetration between donor and acceptor in high-boiling point solvents took a longer time, while the inverse was true in low-boiling point solvents. Therefore, it is also possible to fine-tune the vertical structure and film morphology by tailoring the acceptor solvent.[75] Furthermore, manipulating the components in processing solvent to further tune the interdiffusion makes a well-defined crystallinity gradient distribution and pathway in the active layer, which can assist charge transport and collection in devices, and enable commendable thick-film OSC PCEs (16.0% for 500 nm).[76] Doping strategies can also be used in LbL processing to improve device performance.[77] If dopant molecules can only diffuse in a specific phase, the blend-cast BHJ method cannot segregate the dopant to a single phase, resulting in increased recombination. However, in LbL processed P-BHJ devices dopant molecules can be added to a specific phase before deposition by incorporating into the donor or acceptor solution. Bo et al.[78] used poly(9-vinylcarbazole) (PVK) as an n-type dopant in

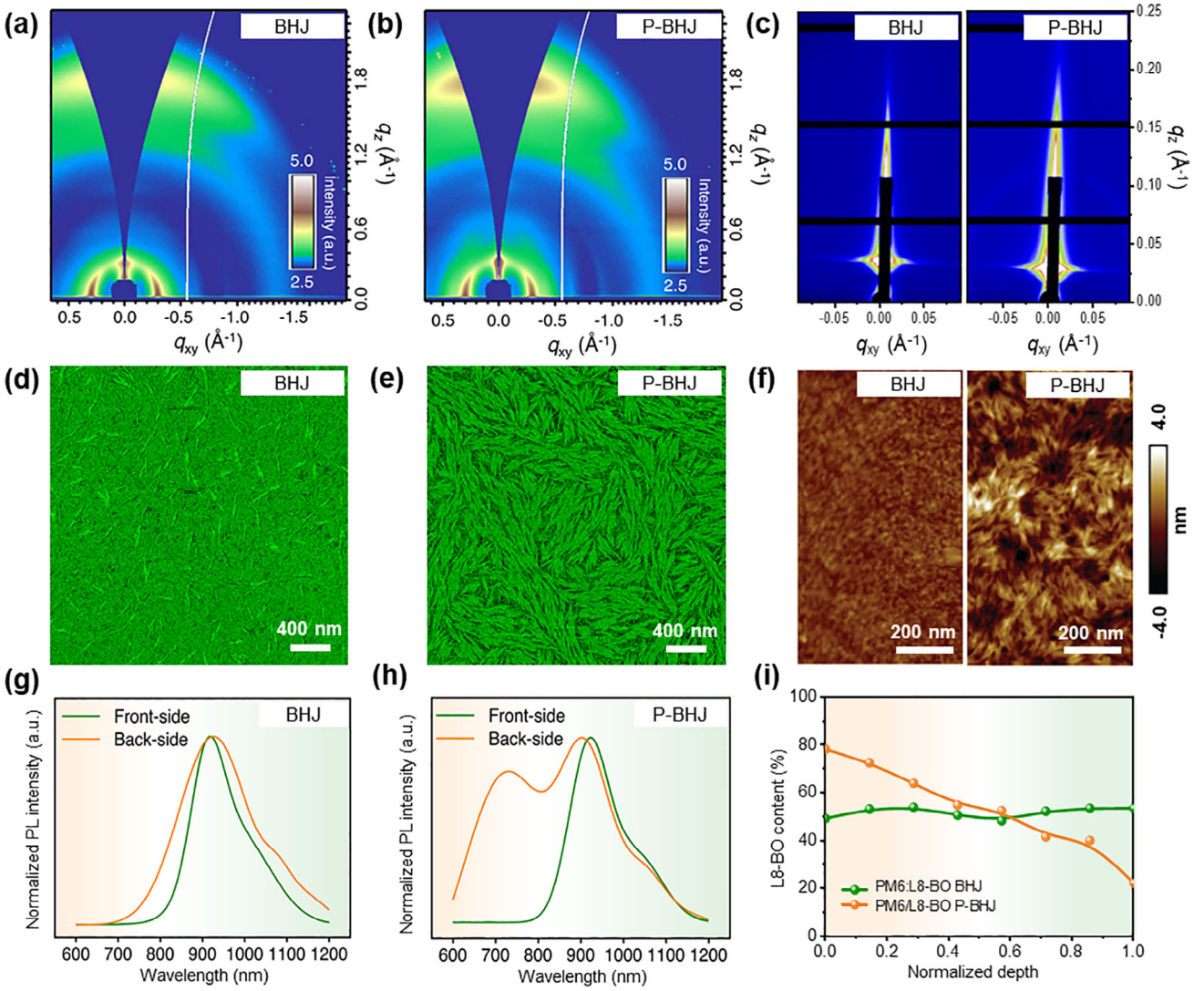

Figure 3. Morphology characterizations. 2D GIWAXS patterns of PM6:N3:PC_{71} BM films with a) BHJ and b) P-BHJ architectures. (Reproduced with permission.[70] Copyright 2021, Springer Nature). c) 2D GISAXS patterns of D18:L8-BO with BHJ and P-BHJ architectures. Photo-induced force microscope (PiFM) images of d) D18:L8-BO BHJ and e) D18/L8-BO P-BHJ films imaged at 1532 cm^{-1} for screening L8-BO. (Reproduced with permission.[59] Copyright 2023, Wiley-VCH). f) AFM images of the BHJ and P-BHJ films. (Reproduced with permission.[71] Copyright 2022, Wiley-VCH). The PL spectra of the film with g) BHJ and h) P-BHJ architectures. (Reproduced with permission.[70] Copyright 2021, Springer Nature). i) Depth profiles from XPS measurements of PM6:L8-BO BHJ and PM6/L8-BO P-BHJ. (Reproduced with permission.[72] Copyright 2024, Springer Nature).

the electron acceptor layer to enhance charge transport and exciton diffusion, thereby improving the efficiency of LbL processed OSCs. They further demonstrated a layered solid additive strategy in LbL processed OSCs, where $FeCl_3$ enhances hole transport in the donor layer and PFO improves morphology in the acceptor layer, thereby optimizing charge transport and suppressing recombination to yield improved device efficiency.[79]

3. Device Physics of P-BHJ OSCs

The sequential film deposition allows for a gradual structure with a p-i-n effects in the active layer, which has the potential to improve the exciton and charge dynamics, and ultimately enhance device performance.[80]

3.1. Exciton Generation and Diffusion

Through precisely controlling the morphology and vertical distribution during LbL processing, more ordered heterojunctions with improved molecular packing can form. These structures lead to pronounced changes in optical properties with slight redshift absorption spectra and higher absorption coefficients, suggesting enhanced photon conversion and exciton generation in P-BHJ films.[70] **Figure** 4a,b show absorption rates calculated from measured optical constants in both BHJ and P-BHJ structures of PM6 and Y6 system, with the P-BHJ exhibiting a superior absorption profile to the BHJ for this system.[81] Further, this demonstrates the differences in film morphology between BHJs and P-BHJs, as mentioned in the previous section.

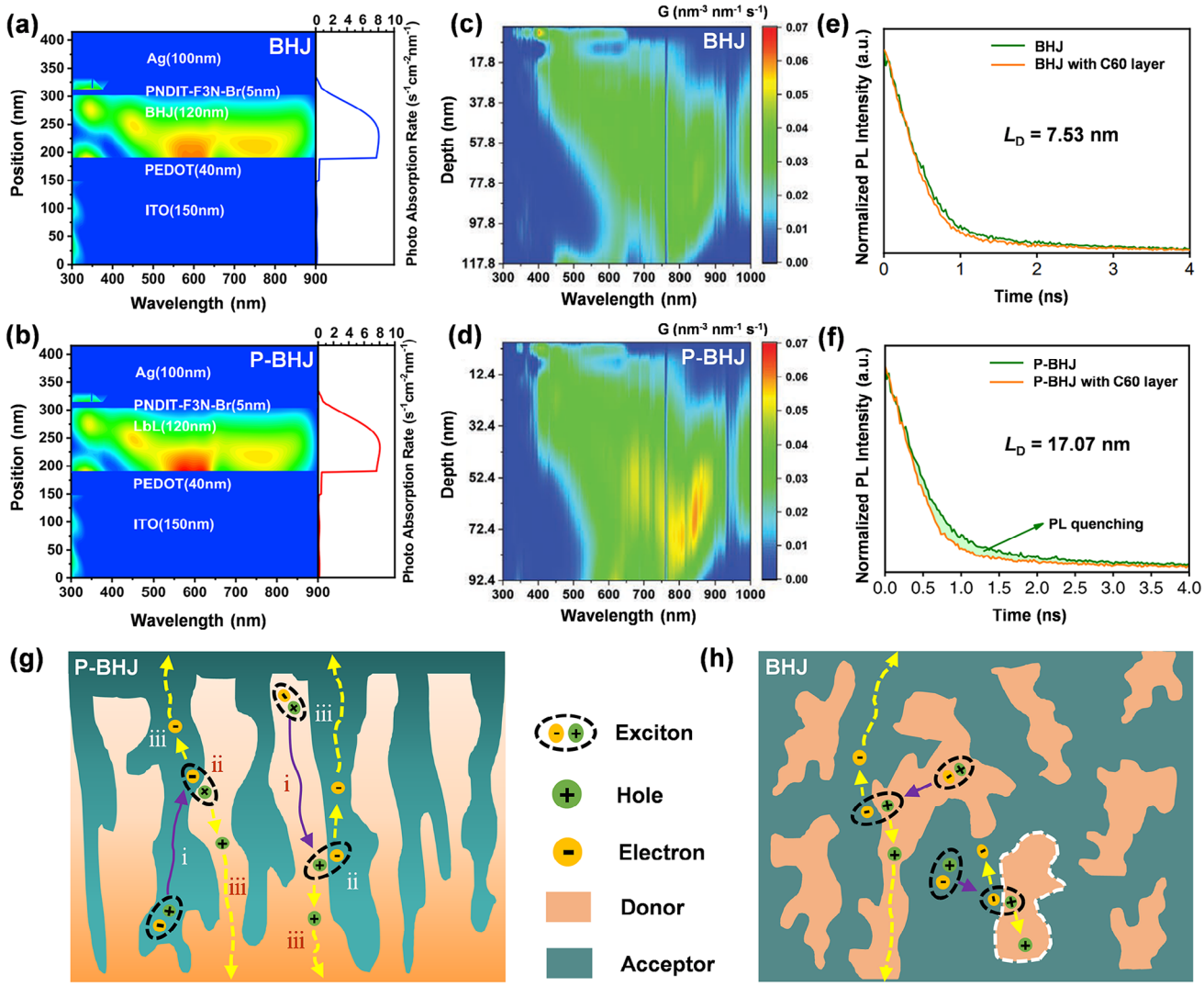

Figure 4. Simulated photo-absorption rate in a) BHJ and b) P-BHJ based OSCs with an active layer thickness of 120 nm. (Reproduced with permission.[81] Copyright 2020, Elsevier). Calculated exciton generation contours in c) BHJ and d) P-BHJ films. (Reproduced with permission.[52] Copyright 2022, Wiley-VCH). PL quenching for e) BHJ and f) P-BHJ films coated with C60 layer. (Reproduced with permission.[70] Copyright 2021, Springer Nature). Schematic outline of g) P-BHJ and h) BHJ active layer structures and corresponding carrier process.

Film-depth-dependent light absorption spectra (FLAS) analysis provides valuable insights into the differences in vertical distribution within BHJ and P-BHJ films. Figure 4c,d depict the distribution of exciton generation rate within devices employing PM6:L8-BO active layers, which were numerically simulated based on the FLAS data in conjunction with a modified transfer-matrix optical model,[82] showing that longer wavelengths of light can penetrate deeper into the active layer and generate excitons near the bottom contact in the P-BHJ devices. It was suggested that the exciton generation rate in the P-BHJ film, surpassing that of the traditional BHJ film across the 600 to 900 nm range, and manifesting as enhancements in external quantum efficiency (EQE) and J_{SC}.[52]

As presented in Figure 4g, after absorbing photons to generate excitons within the active layer, the excitons first (i) diffuse to the donor/acceptor interface, then (ii) form a charge-transfer state by transferring the electron (hole) from the donor (acceptor) to the acceptor (donor) phase, and (iii) dissociate into free charge carriers which are then transported to the corresponding electrodes. The generated excitons in LbL processed P-BHJ active layers can have efficient dissociation due to the long-diffusion length excitons.[70,83] The efficiency of exciton dissociation is contingent upon the morphology and characteristics of the blend, including the formation of an interpenetrating network. Jen et al.[70] proposed that longer exciton diffusion lengths exist in the domains of P-BHJ films, benefiting from enhanced film morphology with a p-i-n effect. A longer exciton diffusion length (L_D) of 17.07 nm was observed in P-BHJ compared to the BHJ counterpart (L_D = 7.53 nm), and this extended exciton diffusion distance enhances exciton dissociation efficiency in the active layer, suggested to contribute to boosting the efficiency of LbL devices to 17.42%. Conversely, the shorter exciton

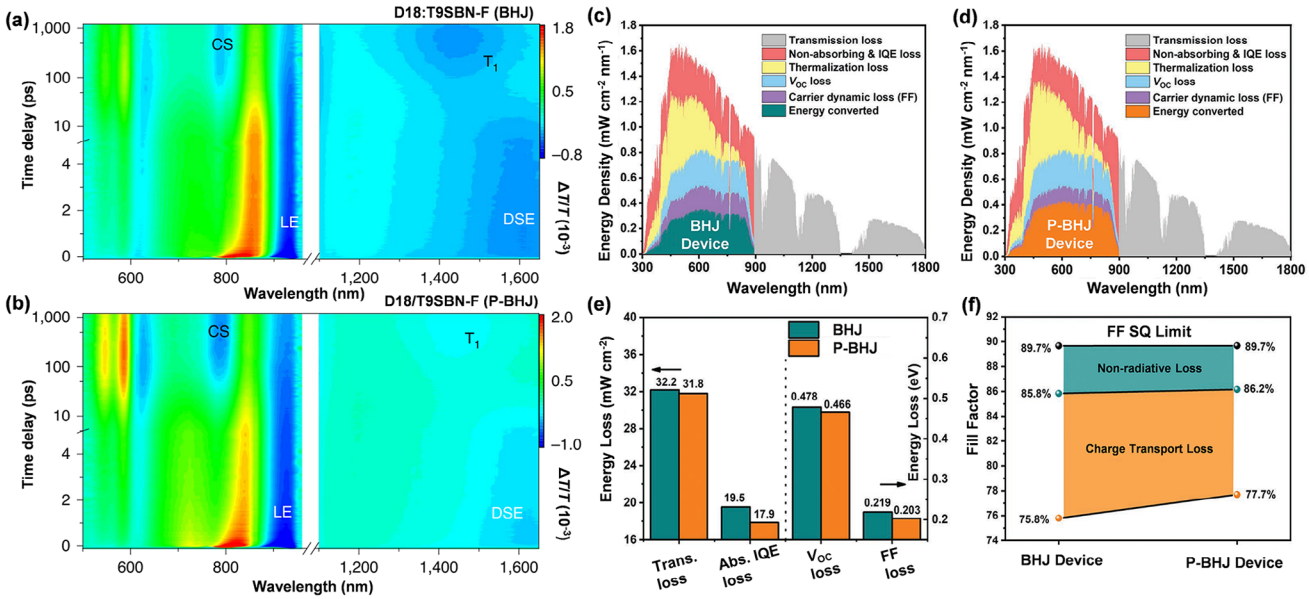

Figure 5. Transient absorption (TA) profiles of a) D18:T9SBN-F BHJ and b) D18/T9SBN-F P-BHJ films. (Reproduced with permission.[74] Copyright 2022, Springer Nature). Detailed total energy loss analysis for the c) BHJ device and d) P-BHJ device based on the illumination of AM 1.5 G, 100 mW cm^{-2}. e) The corresponding Transport loss, Absorption and internal quantum efficiency (IQE) loss, V_{OC} loss, and FF loss. f) The FF in the Shockley-Queisser (SQ) limit[89] consists of charge-transport loss and nonradiative loss of the optimized BHJ device versus the P-BHJ device, respectively. (Figure reproduced with permission from,[71] Copyright 2022, Wiley-VCH).

diffusion length in the domains of PM6:N3:PC_{71} BM BHJ active layer substantially limits their efficiency to 16.44%. The increased diffusion lengths observed in NFAs enable excitons generated in the acceptor phase to diffuse across larger domains, without sacrificing charge generation efficiency. Longer diffusion lengths have been observed in P-BHJ active layers than BHJ counterparts.[62]

3.2. Charge Dynamics and Recombination Loss

A needle-like gradual P-BHJ may help to avoid the formation of both non-intercalated domains and direct contact between the anode (cathode) electrode and the acceptor (donor) component (as per Figure 4g),[84] respectively improving charge transport and collection and reducing unwanted surface recombination (i.e., the extraction of minority carries by the electrodes). It has been suggested that the optimized gradual interface and vertical phase distribution can reduce energetic disorder, leading to a narrower DOS; as a result, the corresponding electron quasi-Fermi level (E_{Fn}) and hole quasi-Fermi level (E_{Fp}) in the P-BHJ can ultimately be up-shifted and down-shifted, respectively, reducing disorder-induced V_{OC} loss.[85] Through analyzing the photoexcited local excitons (LE), delocalized singlet excitons (DSE) and charge-separated (CS) state (see **Figure** 5a,b), it was demonstrated that due to the spin character of charge-transfer states, recombining charge carriers are most likely to form the lowest-energy triplet exciton (T1), leading to non-radiative photocurrent loss. P-BHJ active layers alleviate this loss with improved phase separation that increases the rate of interfacial charge-transfer state dissociation while suppressing non-geminate recombination events. This suppression lowers the probability of T1 formation and thus limits the change of relaxation through this state.[74] Furthermore, the more defined donor and acceptor domains in P-BHJs facilitate more efficient charge extraction before non-geminate recombination occurs, further reducing triplet exciton formation.

More insightful analysis can be obtained through the device physical parameters. As depicted in Figure 5c,d, P-BHJ devices exhibit higher charge generation efficiencies than in their BHJ counterparts, consistent with the higher PCE of P-BHJ devices. There is a reduced transmission loss (Tran. Loss in Figure 5e) in P-BHJ OSCs, which can be attributed to the slight redshift in absorption through LbL processing. Benefiting from the P-BHJ active layer structure to improve exciton dissociation rate and separation efficiency, the absorption and IQE losses (Abs. IQE loss in Figure 5e) are reduced from 19.5 mW cm^{-2} for the BHJ device to 17.9 mW cm^{-2} for the P-BHJ device. Owing to enhanced light absorption and improved exciton diffusion, the P-BHJ OSCs exhibit lower energy loss in which V_{OC} loss is smaller than the BHJ as mentioned above, and the regular packing and higher order structure in P-BHJ device may also suppress molecular vibration and non-radiative recombination, resulting in reduced V_{OC} loss.[86] It was also suggested that a reduction in non-radiative loss occurs due to a suppressed trap-assistant recombination in the P-BHJ film morphology: while the enhanced and more balanced carrier mobilities in the P-BHJ active layer reduced charge transport loss and resulted in higher FF (see in Figure 5f).[87,88] Additionally, it has been reported that LbL devices possess smaller series resistance (R_s) and larger shunt resistance (R_{sh}), which is also beneficial to charge collection and achieving higher FFs.[71]

3.3. Computational Approaches and Analyses

Computational approaches have, for decades, been a cornerstone of research into OSCs, with a plethora of methods being employed to explore the effect of active layer morphology at various length scales. In these approaches, morphological properties such as molecular packing and energetic disorder have been investigated, as well as kinetic charge generation processes such as exciton migration and separation (via interfacial charge-transfer state formation), and charge separation, transportation, and extraction. Considering these processes at the molecular scale provides a window into how interactions between excited molecules can ultimately define the performance of OSCs.

Usually, different computational approaches are applicable to different length scales in OSCs, with multiscale simulations often combining several approaches for a holistic view of the charge generation process.[90] At the smaller scales, the geometry, arrangement, and packing of molecules can be explored using techniques such as molecular dynamics (MD) simulations, which can provide insights into the energetic disorder of the donor and acceptor phases,[91] with reduced energetic disorder generally correlating with reduced open-circuit voltage losses,[92] and higher OSC performance.[93,94] Similar techniques such as time-dependent density functional theory (DFT) simulations can also provide insight into the structure, crystallinity, and excited states energies of molecules.[95] DFT-based simulations can be used to estimate the energy levels of the highest-occupied molecular orbital (HOMO) and the lowest-unoccupied molecular orbital (LUMO) of the donor and the acceptor molecules,[96] as well as the couplings between excitons and CT states.[97–100] Though it should be noted that the HOMO and LUMO energy levels obtained using DFT approaches are primarily for molecules in the gas phase.[101] These values appear to be determined more accurately using techniques such as ultraviolet photoelectron spectroscopy and cyclic voltammetry.[101,102] The differences between these energetic levels for donor and acceptor molecules, alongside the associated couplings, will influence the rate of kinetic processes like electron transfer from donor to acceptor and hole transfer from acceptor to donor.[7]

Approaches that model individual molecules such as MD and DFT generally become computationally expensive at the device scale, where the number of molecules and their interactions becomes too large.[99] At these scales, the phase separation and distribution of donor and acceptor regions in the active layers of BHJs (and the intermixed region of P-BHJ devices) can instead be simulated using less-detailed, numerical techniques such as the Ising model,[103,104] in which the active layer is discretized into a lattice of sites with discrete spins that align as the simulation time progresses. Though these techniques lack the nuance of atomistic and MD approaches as they neglect the interactions between molecules.

Once a distribution of donor and acceptor sites and an associated energetic and kinetic landscape have been established, other in-silico approaches can be used to characterize the performance of OSCs. One such example that, for decades, has been applied extensively are kinetic Monte Carlo (kMC) simulations,[105–107] which can predict resultant parameters such as the bimolecular recombination rate constant and mobility, while accounting for nanoscale couplings between sites, polaronic effects, and spatially-decaying probabilities.[108,109] Generally, the portrayal of the charge transport process in disordered OSCs offered by kMC approaches is more accurate than macroscale approaches like finite element drift-diffusion modelling or equivalent circuit models, though it comes at the cost of higher computational expense.[108]

Multiscale approaches have been somewhat used to explore the benefits of P-BHJ morphology or similar. Predominantly, optical simulations have been used to investigate the differences between the P-BHJ and the BHJ morphologies,[81,110] though investigations accounting for the energetics and kinetics proffered by different morphologies have been conducted.[111] An investigation on the effect of non-thermalized – or hot – excitons was also carried out by Upreti et al. using a funneled active layer morphology,[112] which resembles the P-BHJ in its p-i-n like structure (with acceptors near the cathode and donors near the anode); as previously mentioned, this structure could enhance carrier utilization efficiency.[69,73]

In years to come, multiscale approaches will continue to further the community's understanding of how the arrangement of molecules and their excited states will impact the performance of OSCs, wherein morphological considerations such as molecular stacking, orientation, and composition, can be combined with optical considerations and larger-scale device models, such as drift-diffusion.

3.4. Device Stability

OSCs often face stability issues due to the diffusion of molecules of various layers under heat and light stress.[85] The initial phase-separated morphology can be compromised as the materials self-aggregate, forming too large domains that degrade the performance of the OSCs.[113] This can be partially mitigated in LbL processed P-BHJ OSCs with optimized heterojunction absorbers, which are inherently more robust due to improved donor/acceptor phase separation with more interface area. Additionally, these OSCs provide a window to optimize the assembly of the materials before making devices, rather than directly blending materials without treatment, resulting in enhanced morphological control. By precisely controlling interfacial properties and intermixing between donor and acceptor materials, LBL film processing can achieve more ordered heterojunctions and optimized phase separation,[13,29] thus increasing the thermodynamic stability, reducing the degradation process, and enhancing device stability. Some materials used in OSCs tend to form large aggregates in the active layer over time, which worsens the morphology.[114] The enhanced stability of P-BHJ OSCs demonstrates superior long-term photostability and thermal stability compared to conventional BHJ OSCs. Morphological studies of both fresh and aged films via optical microscopy (OM) and AFM indicate that P-BHJ structures are far more resilient than their BHJ counterparts. As illustrated in **Figure 6**a,b, aged BHJ films exhibit micron-scale phase separation and excessive segregation in donor and acceptor domains. In contrast, P-BHJ films display considerably less morphological degradation under both photo and thermal stress. As we can see in Figure 6c,g, the LbL processed P-BHJ film has not changed significantly after photo annealing, exhibiting robust morphological stability.

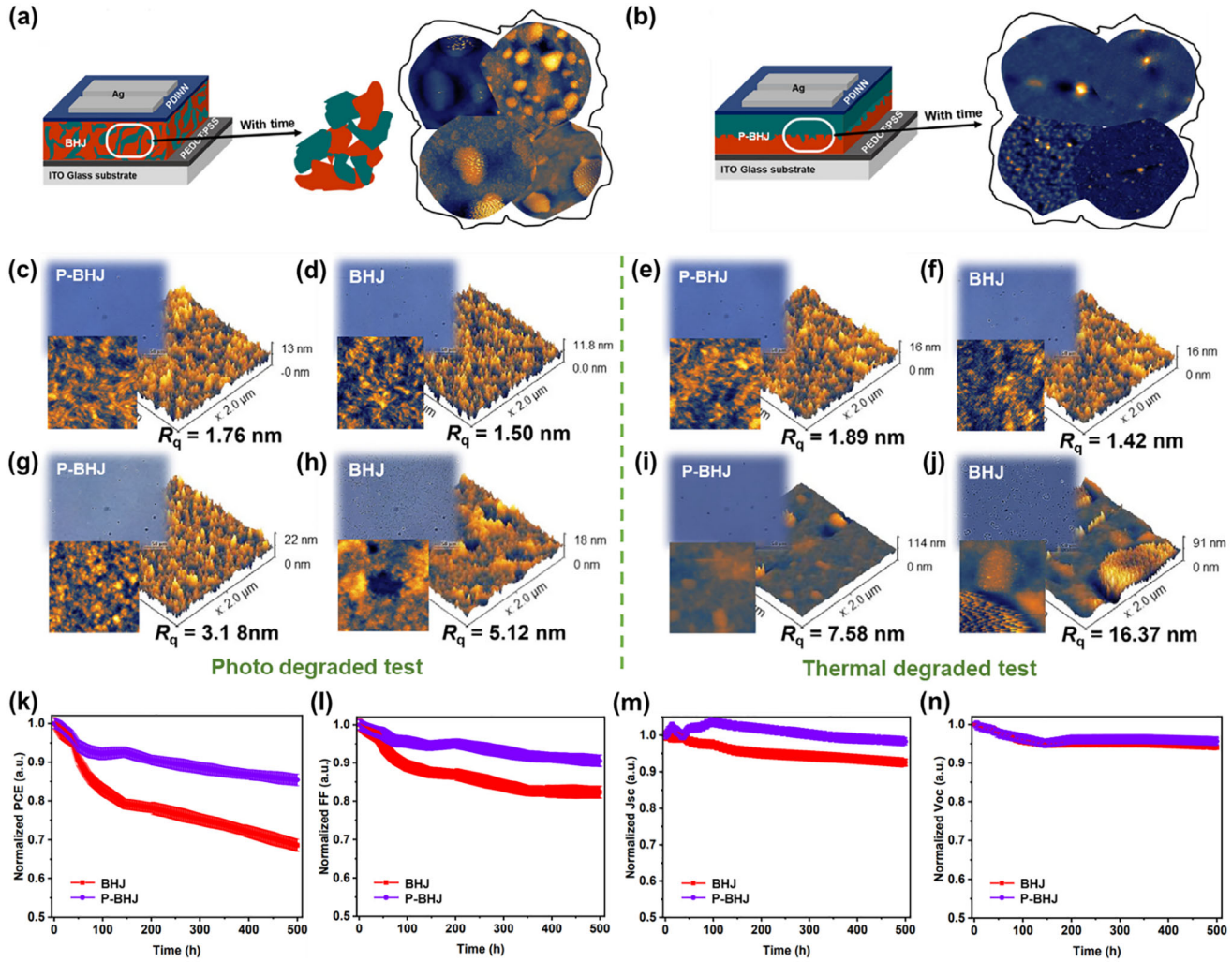

Figure 6. Morphological comparison and long-term stability of P-BHJ and BHJ. Comparison of phase aggregation in a) BHJ and b) P-BHJ architectures; Corresponding OM and AFM images of fresh c, e) P-BHJ films and d, f) BHJ films. Morphological comparison of photo degraded g) P-BHJ and (h) BHJ films and thermal degraded i) P-BHJ and j) BHJ films. (Reproduced with permission.[115] Copyright 2024, Elsevier). k-n) Normalized V_{OC}, J_{SC}, FF, and PCE values versus illumination time over 500 h for the BHJ and P-BHJ based OSCs. (Reproduced with permission.[85] Copyright 2019, The Royal Society of Chemistry).

However, the traditional BHJ film shows obvious film morphological evolution, which can be seen from the dots in the OM images and the high roughness changes in the AFM images in Figure 6d,h, reflecting the weak morphological photostability of the traditional BHJ film. Further thermal stability tests in Figure 6f,j show that the traditional BHJ film will undergo severe morphological changes, which may be the reason why the BHJ device performance shows poor thermal stability. Although the P-BHJ film also suffers morphological changes, these are generally much milder compared to the BHJ film (see Figure 6e,i). Owing to the slower degradation, a smaller long-term PCE loss is obtained in P-BHJs, relative to their corresponding BHJ counterparts as observed across eight other non-fullerene acceptor (NFA) systems.[115]

The stability comparison of specific photovoltaic parameters in BHJ and P-BHJ devices is worthy of study and provides considerable insight. Figure 6k-n shows the changes of photovoltaic parameters of the OSCs,[85] where the P-BHJ device is more stable than the BHJ; the PCE degrades down to 68% of its initial vale within 500 h in the BHJ but only 85% in P-BHJ. In particular, the J_{SC} and FF in the BHJ show the most notable drop (Figure 6k), while the FF and J_{SC} stabilities of P-BHJ OSCs are comparably more stable, which may be attributed to the improved active layer structure and more stable morphology. It is worth noting that from Figure 6n, it can be found that the V_{OC} of BHJ and P-BHJ OSCs are nearly the same, which suggests the interfaces are well designed and the contacts optimized in both cases. In addition, P-BHJ devices also show better thermal stability than BHJ with the morphology barely changing after heating at 120 °C for 1500 h in this case.[85]

To inhibit disordered molecular diffusion, which typically results in the loss of crystallinity in acceptor domains, a third component is commonly introduced: for instance, a guest acceptor can create an alloy-like acceptor with the host acceptor.[116,117]

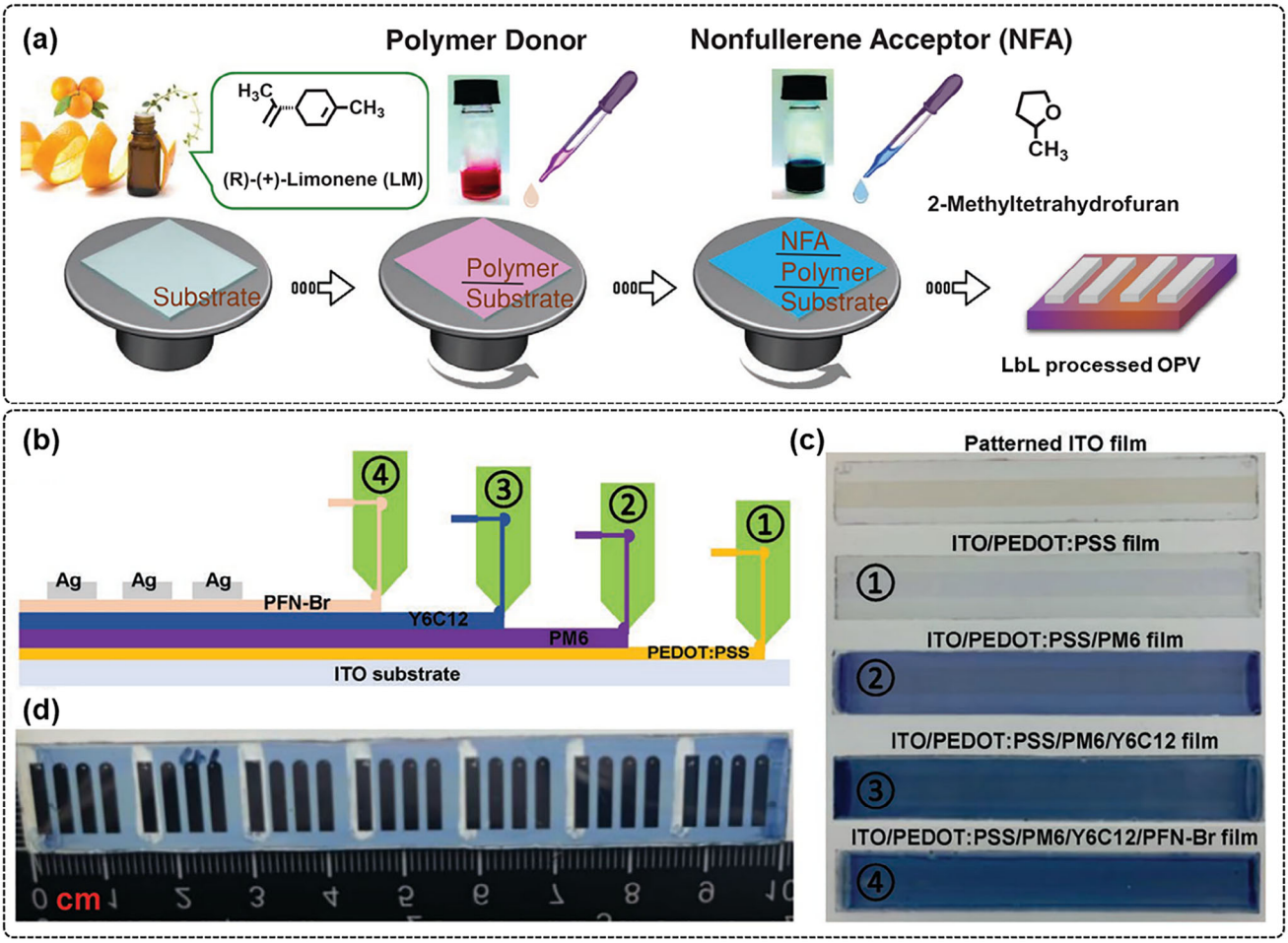

Figure 7. Potential in device fabrication. a) Illustration of eco-friendly sequential deposition protocol for devices fabrication. (Reproduced with permission.[124] Copyright 2019, Wiley-VCH). b) Visual schematic of the LbL slot-die coated. c) Camera images of the patterned ITO-coated glass substrate (10 cm strip), and the different slot-die-coated films from the bottom layer (PEDOT:PSS film) to the top layer (PFN-Br film) under ambient conditions. d) Camera image of the slot-die coated device after the silver electrode deposition. (Reproduced with permission.[126] Copyright 2023, Wiley-VCH).

These alloy-like acceptors enhance the crystallinity of the acceptor phase by promoting more ordered molecular packing, effectively suppressing the loss of NFA crystallinity caused by molecular diffusion during illumination, which enhances morphological stability under operation.[117] In addition, introducing another donor or acceptor into the different layers of the donor and acceptor, respectively, is also a good way to realize an ideal and stable active layer morphology.

4. Future Directions and Applications

LBL processing of donor and acceptor materials into P-BHJs creates well-defined pathways for charge transport, minimizes recombination sites, and has the potential to improve charge mobility and collection. Moreover, the enhanced thermodynamic stability of the P-BHJ structure improves the device stability of OSCs, vital for productization. OSCs have recently achieved high PCEs at the small-area scale (cm^2), while current research aims to tackle the challenge of extending these efficiencies to larger areas and module scales.[118,119] LbL processing not only holds the promise of bridging the gap from small-scale to module-scale, but could also be helpful for the fabrication of stable OSCs.

4.1. Eco-Friendly Fabrication

Nonhalogenated solvents are preferrable for the industrial-scale production of large-area OSCs, owing to their minimal toxicity.[120,121] In the fabrication of P-BHJ devices, the consideration of component ratios and co-processing solvents is unnecessary, making the process conducive for operation both in laboratory and industrial settings, particularly well-suited for the manufacture of large-area devices.[122] Yan et al.[123] reported the utilization of eco-friendly solvents to fabricate OSCs achieving efficiencies exceeding 19% through incorporating the auxiliary film treatment in the gap between donor and acceptor in LbL processing, positioning LbL processing as a promising strategy in green-solvent processed OSCs. As displayed in **Figure 7a**, using the solvents (R)-(+)-limonene (LM) and 2-Methyltetrahydrofuran in the LbL allows for OSCs that are both ecofriendly and can be derived

from renewable bio sources.[124] Furthermore, water has even been used as a solvent in the preparation of polymer donor components of P-BHJ devices, which achieve a PCE of 19%, though the acceptor still used an organic solvent.[125]

4.2. Large-Area Devices

Devices fabricated through LbL blade coating exhibit enhanced PCE compared to those produced via blended blade coating and show the versatility of the LbL coating method after comparing multiple systems. This LbL strategy was further extended to prepare device modules with larger photoactive areas. Notably, the PCE of the P-BHJ device module, with an effective area of 11.52 cm^2, reached 11.86%, surpassing the BHJ device efficiency of 10.15%.[81] Figure 7b shows the use of slot-die to coat hole transport layer (PEDOT:PSS), LbL processed active layer (with PM6 and Y6C12 coating in sequence), and electron transport layer (PFN-Br). As indicated in the image of film in each step shown in Figure 7c, the good film morphology supports the feasibility of this preparation method; the corresponding all slot-die coated OSC (see in Figure 7d) using eco-friendly solvents in ambient conditions reached a PCE of 10.6%.[126] This not only demonstrates the unique advantages of the LbL processing strategy but also underscores its potential, easy fabrication, and enhanced process engineering, making it suitable for large-area device fabrication and roll-to-roll printing.

4.3. Flexible OSCs

Achieving high efficiency while maintaining mechanical robustness remains a challenge for OSCs. LbL processing shows high potential in developing highly stable and efficient flexible OSCs (FOSCs), which enables precise control over the vertical phase distribution and well-ordered donor-acceptor domains. These advantages are beneficial for flexible devices, as they minimize morphological degradation under mechanical stress. Owing to more stable morphology, FOSCs based on PET/ITO/PEDOT:PSS/active layer/PDINO/Al retained 92% of the initial PCE after 2000 bending cycles in P-BHJ devices, compared to 85% in BHJ devices.[85] Moreover, LbL processed OSCs enable separate depositing of the donor and acceptor with solvent orthogonality and multi-selectivity, which is vital for preparing films on flexible substrates. By tuning the mechanical properties of each layer through material selection and processing control, LbL processing can further improve device flexibility while maintaining high PCEs. It has demonstrated that FOSCs fabricated via LbL processing exhibit lower crack propagation and enhanced stretchability compared to their BHJ counterparts,[127] suggesting the potential in developing high efficient FOSCs for next-generation wearable devices, foldable electronics, and portable solar chargers. In addition, it utilizes eco-friendly solvents and scalable processes, ensuring that FOSCs can be manufactured on large areas while preserving their high PCE.

4.4. Application-Targeted Photovoltaics

As LbL processed OSCs offer refined control of film morphology and optimized performance over BHJ approaches, they are promising for many photovoltaic applications. For example, one promising application is developing printable solar windows, which require devices that optimize light absorption while maintaining transparency. By fine-tuning the donor-acceptor composition and thickness via LbL techniques, it is possible to fabricate OSCs with high transparencies at different wavelengths (i.e., different colors), making them a great candidate for applying in windows and building-integrated photovoltaics (BIPV) without significantly compromising efficiency. Furthermore, scalable fabrication approaches compatible with eco-friendly, non-halogenated solvents ensure that large-area modules for BIPV can be manufactured reliably. Chen et al.[128] found the LbL processed OSCs showed less optical loss and higher average visible transmittance (AVT) value than that of counterpart, and their improved D-A interfaces and optimized active layer morphology reduced the light scattering and parasitic absorption, which helped to improve light utilization when adopted in solar windows. Integrating LbL processing with strategies to enhance stability can enable better applications of BIPVs. They incorporated the superhydrophobic patterned soft insertion layer (PSIL) into double-glass encapsulation can avoid the loss of AVT and provide long-term waterproof performance.

Another application of OSCs that would benefit from the higher PCEs offered by LbL approaches is agrivoltaics, wherein semi-transparent photovoltaics are integrated into agricultural settings such as greenhouses and polytunnels,[129,130] thereby optimizing land-use while providing locally-generated power. By fine-tuning factors such as the thickness of active layer (and of the donor-acceptor regions using LbL techniques), the AVT of the OSCs can be optimized to match the wavelength requirements of any crops below.[130–132] This of course comes with the caveat that the OSCs must transmit (i.e., not absorb) some visible light and thus generate less power. The optimization of agrivoltaic systems (consisting of the photovoltaics and the crops) is therefore a multi-variable challenge requiring a delicate balance between power generation and maintaining high crop yields. Nevertheless, the tunable transmittances and optical gaps of OSCs make them desirable for this application.

Another application of OSCs that has gained considerable traction in recent years is indoor photovoltaics,[133–135] in which low-intensity ambient light is harvested to power sensors and communications devices belonging to the Internet-of-Things (IoT). Once again, the tunable optical gaps of OSCs make them particularly desirable as indoor lighting conditions are diverse, with LEDs, fluorescent lamps, sunlight, or some superposition of the above being present in many internal spaces.[136,137] These different light sources have unique spectral distributions, which can affect device performance. For example, at a fixed light intensity a “warm-white” LED has more red photons than a “cool-white” LED, meaning that the PCE of organic photovoltaics with a given optical gap can change depending on its light source.[138] For most indoor light sources, OSC materials with an optical gap between 1.7 and 1.9 eV are desirable.[93] Using these materials, indoor photovoltaics only need device areas on the order of 30 cm^2 to power most IoT devices,[139] thereby removing the need for disposable batteries and wires, reducing waste, and minimizing maintenance costs.

5. Summary

The development of LbL processed P-BHJ OSCs has exhibited significant improvement and potential, including device PCE, stability and scaling. This illustrates that film-process advancements and morphological control are undoubtedly the key to fabricating high-performance stable OSCs. LbL processing offers flexible morphological control strategies, providing more approaches for manipulating molecular packing and aggregation within the donor and acceptor phases, resulting in more optimized exciton dynamics and charge transport. Simultaneously, the enhanced p-i-n vertical distribution and gradual interface in P-BHJ active layer can facilitate efficient charge collection and reduced recombination loss in devices, with the added benefit of improved device stability. Furthermore, compared to traditional BHJ active layers, P-BHJ active layers demonstrate less morphological degradation, good bending tolerance, flexible film processing methods, and have shown promise in large-area slot-die coating. Couple this with the potential for greener device fabrication and LBL processing is expected to become essential for the next evolution in OSC fabrication. LbL processing is applicable to ternary, perovskite/organic tandem solar cells and organic photodetectors. Although there are some processing complexities in the fabrication of P-BHJ OSCs and inverted devices, solving these may become the next research direction in P-BHJ OSCs. Through further study, LbL processed P-BHJ devices can act as promising candidates for developing efficient, stable and scalable OSCs, making a considerable advance in OSCs fabrication, with improved device performance and environmental fabrication to address efficiency-stability trade-offs S1.

Supporting Information

Supporting Information is available from the Wiley Online Library or from the author.

Acknowledgements

This work was supported by the Welsh Government's Sêr Cymru II Program through the European Regional Development Fund, Welsh European Funding Office, and the Swansea University strategic initiative in Sustainable Advanced Materials. A.A. was a Sêr Cymru II Rising Star Fellow, and P.M. is a Sêr Cymru II National Research Chair. O.J.S. is an Academy Research Fellow and acknowledges funding from the Research Council of Finland through project #357196. This work was also funded by UKRI through the EPSRC Program Grant EP/T028513/1 Application Targeted Integrated Photovoltaics and Centre for Integrative Semiconductor Materials (UKRI Research Partnership Investment Fund).

Conflict of Interest

The authors declare no conflict of interest.

Author Contributions

D.L.– Conceptualization, methodology, formal analysis, investigation, data curation, writing – original draft, and visualization. A.M.K.– Methodology, formal analysis, investigation, writing – original draft. D.B.R.– investigation, writing – review and editing. O.J.S.– Investigation, writing – review, and editing. A.A.– Writing – review and editing, supervision. P.M.– Resources, writing – review and editing, supervision, project administration, and funding acquisition.

Keywords

layer-by-layer, organic solar cells, power conversion efficiency, pseudo-bilayer heterojunctions, stability

Received: February 10, 2025
Revised: March 26, 2025
Published online:

[1] P. Meredith, W. Li, A. Armin, *Adv. Energy Mater.* **2020**, *10*, 2001788.
[2] A. Armin, W. Li, O. J. Sandberg, Z. Xiao, L. Ding, J. Nelson, D. Neher, K. Vandewal, S. Shoaee, T. Wang, H. Ade, T. Heumüller, C. Brabec, P. Meredith, *Adv. Energy Mater.* **2021**, *11*, 2003570.
[3] L. Zhu, M. Zhang, J. Xu, C. Li, J. Yan, G. Zhou, W. Zhong, T. Hao, J. Song, X. Xue, Z. Zhou, R. Zeng, H. Zhu, C. C. Chen, R. C. I. MacKenzie, Y. Zou, J. Nelson, Y. Zhang, Y. Sun, F. Liu, *Nat. Mater.* **2022**, *21*, 656.
[4] Y. Jiang, S. Sun, R. Xu, F. Liu, X. Miao, G. Ran, K. Liu, Y. Yi, W. Zhang, X. Zhu, *Nat. Energy* **2024**, *9*, 975.
[5] Y. Sun, L. Wang, C. Guo, J. Xiao, C. Liu, C. Chen, W. Xia, Z. Gan, J. Cheng, J. Zhou, Z. Chen, J. Zhou, D. Liu, T. Wang, W. Li, *J. Am. Chem. Soc.* **2024**, *17*, 51.
[6] C. Li, G. Yao, X. Gu, J. Lv, Y. Hou, Q. Lin, N. Yu, M. S. Abbasi, X. Zhang, J. Zhang, Z. Tang, Q. Peng, C. Zhang, Y. Cai, H. Huang, *Nat. Commun.* **2024**, *15*, 8872.
[7] O. J. Sandberg, A. Armin, *J. Phys. Chem. C* **2021**, *125*, 15590.
[8] X. Lu, C. Xie, Y. Liu, H. Zheng, K. Feng, Z. Xiong, W. Wei, Y. Zhou, *Nat. Energy* **2024**, *9*, 793.
[9] Z. Bi, W. Ma, *Matter* **2020**, *2*, 14.
[10] G. Li, R. Zhu, Y. Yang, *Nat. Photonics* **2012**, *6*, 153.
[11] C. W. Tang, *Appl. Phys. Lett.* **1986**, *48*, 183.
[12] G. Yu, J. Gao, J. C. Hummelen, F. Wudl, A. J. Heeger, *Science* **1995**, *270*, 1789.
[13] L. Zhu, M. Zhang, G. Zhou, Z. Wang, W. Zhong, J. Zhuang, Z. Zhou, X. Gao, L. Kan, B. Hao, F. Han, R. Zeng, X. Xue, S. Xu, H. Jing, B. Xiao, H. Zhu, Y. Zhang, F. Liu, *Joule* **2024**, *8*, 3153.
[14] Y. Lin, J. Wang, Z. Zhang, H. Bai, Y. Li, D. Zhu, X. Zhan, *Adv. Mater.* **2015**, *27*, 1170.
[15] J. Yuan, Y. Zhang, L. Zhou, G. Zhang, H. L. Yip, T. K. Lau, X. Lu, C. Zhu, H. Peng, P. A. Johnson, M. Leclerc, Y. Cao, J. Ulanski, Y. Li, Y. Zou, *Joule* **2019**, *3*, 1140.
[16] L. Ding, Z. D. Yu, X. Y. Wang, Z. F. Yao, Y. Lu, C. Y. Yang, J. Y. Wang, J. Pei, *Chem. Rev.* **2023**, *123*, 7421.
[17] T. Chen, S. Li, Y. Li, Z. Chen, H. Wu, Y. Lin, Y. Gao, M. Wang, G. Ding, J. Min, Z. Ma, H. Zhu, L. Zuo, H. Chen, *Adv. Mater.* **2023**, *35*, 2300400.
[18] J. Cheng, C. Guo, L. Wang, Y. Fu, D. Li, C. Chen, Z. Gan, Y. Sun, D. Liu, W. Li, T. Wang, *Joule* **2024**, *8*, 2250.
[19] C. J. Schaffer, C. M. Palumbiny, M. A. Niedermeier, C. Jendrzejewski, G. Santoro, S. V Roth, P. Müller-Buschbaum, C. J. Schaffer, C. M. Palumbiny, M. A. Niedermeier, C. Jendrzejewski, P. Müller-Buschbaum, G. Santoro, S. V Roth, *Adv. Mater.* **2013**, *25*, 6760.
[20] L. Ye, B. A. Collins, X. Jiao, J. Zhao, H. Yan, H. Ade, *Adv. Energy Mater.* **2018**, *8*, 1703058.
[21] M. Ghasemi, N. Balar, Z. Peng, H. Hu, Y. Qin, T. Kim, J. J. Rech, M. Bidwell, W. Mask, I. McCulloch, W. You, A. Amassian, C. Risko, B. T. O'Connor, H. Ade, *Nat. Mater.* **2021**, *20*, 525.
[22] N. Li, J. D. Perea, T. Kassar, M. Richter, T. Heumueller, G. J. Matt, Y. Hou, N. S. Güldal, H. Chen, S. Chen, S. Langner, M. Berlinghof, T. Unruh, C. J. Brabec, *Nat. Commun.* **2017**, *8*, 14541.
[23] Y. Diao, L. Shaw, Z. Bao, S. C. B. Mannsfeld, *Energy Environ. Sci.* **2014**, *7*, 2145.

[24] P. Wang, J. Zhang, D. Luo, J. Xue, L. Zhang, H. Mao, Y. Wang, C. Yu, W. Ma, Y. Chen, *Adv. Funct. Mater.* **2024**, *34*, 2402680.
[25] X. Xu, W. Jing, H. Meng, Y. Guo, L. Yu, R. Li, Q. Peng, *Adv. Mater.* **2023**, *35*, 2208997.
[26] H. Fu, W. Gao, Y. Li, F. Lin, X. Wu, J. H. Son, J. Luo, H. Y. Woo, Z. Zhu, A. K. Y. Jen, *Small Methods* **2020**, *4*, 2000687.
[27] L. Wen, H. Mao, L. Zhang, J. Zhang, Z. Qin, L. Tan, Y. Chen, *Adv. Mater.* **2024**, *36*, 2308159.
[28] D. He, J. Zhou, Y. Zhu, Y. Li, K. Wang, J. Li, J. Zhang, B. Li, Y. Lin, Y. He, C. Wang, F. Zhao, *Adv. Mater.* **2024**, *36*, 2308909.
[29] M. T. Sajjad, A. Ruseckas, I. D. W. Samuel, *Matter* **2020**, *3*, 341.
[30] T. H. Lee, Y. Dong, R. A. Pacalaj, S. Y. Park, W. Xu, J. Kim, J. R. Durrant, *Adv. Funct. Mater.* **2022**, *32*, 2208001.
[31] H. Kang, X. Zhang, X. Xu, Y. Li, S. Li, Q. Cheng, L. Huang, Y. Jing, H. Zhou, Z. Ma, Y. Zhang, *J. Phys. Chem. Lett.* **2021**, *12*, 10663.
[32] B. Xiao, M. Zhang, J. Yan, G. Luo, K. Gao, J. Liu, Q. You, H.-B. Wang, C. Gao, B. Zhao, X. Zhao, H. Wu, F. Liu, *Nano Energy* **2017**, *39*, 478.
[33] J. Liu, Y. Zhang, X. Liu, L. Wen, L. Wan, C. Song, J. Xin, Q. Liang, *Small Methods* **2024**, *8*, 2301803.
[34] J. Fu, Q. Yang, P. Huang, S. Chung, K. Cho, Z. Kan, H. Liu, X. Lu, Y. Lang, H. Lai, F. He, P. W. K. Fong, S. Lu, Y. Yang, Z. Xiao, G. Li, *Nat. Commun.* **2024**, *15*, 1830.
[35] Y. Yang, E. Feng, H. Li, Z. Shen, W. Liu, J. Guo, Q. Luo, J. Zhang, G. Lu, C. Ma, J. Yang, *Nano Res.* **2021**, *14*, 4236.
[36] C. Guo, Y. Sun, L. Wang, C. Liu, C. Chen, J. Cheng, W. Xia, Z. Gan, J. Zhou, Z. Chen, J. Zhou, D. Liu, J. Guo, W. Li, T. Wang, *Energy Environ. Sci.* **2024**, *17*, 2492.
[37] J. Yi, G. Zhang, H. Yu, H. Yan, *Nat. Rev. Mater.* **2023**, *9*, 46.
[38] J. Zhao, Y. Li, G. Yang, K. Jiang, H. Lin, H. Ade, W. Ma, H. Yan, *Nat. Energy* **2016**, *1*, 15027.
[39] P. E. Hartnett, A. Timalsina, H. S. S. R. Matte, N. Zhou, X. Guo, W. Zhao, A. Facchetti, R. P. H. Chang, M. C. Hersam, M. R. Wasielewski, T. J. Marks, *J. Am. Chem. Soc.* **2014**, *136*, 16345.
[40] D. Li, X. Zhang, D. Liu, T. Wang, *J. Mater. Chem. A* **2020**, *8*, 15607.
[41] M. Lv, Q. Wang, J. Zhang, Y. Wang, Z. Zhang, T. Wang, H. Zhang, K. Lu, Z. Wei, D. Deng, *Adv. Mater.* **2024**, *36*, 2310046.
[42] C. Li, J. Zhou, J. Song, J. Xu, H. Zhang, X. Zhang, J. Guo, L. Zhu, D. Wei, G. Han, J. Min, Y. Zhang, Z. Xie, Y. Yi, H. Yan, F. Gao, F. Liu, Y. Sun, *Nat. Energy* **2021**, *6*, 605.
[43] S. Dai, J. Zhou, S. Chandrabose, Y. Shi, G. Han, K. Chen, J. Xin, K. Liu, Z. Chen, Z. Xie, W. Ma, Y. Yi, L. Jiang, J. M. Hodgkiss, X. Zhan, *Adv. Mater.* **2020**, *32*, 2000645.
[44] X. Zhang, C. Li, J. Xu, R. Wang, J. Song, H. Zhang, Y. Li, Y. N. Jing, S. Li, G. Wu, J. Zhou, X. Li, Y. Zhang, X. Li, J. Zhang, C. Zhang, H. Zhou, Y. Sun, Y. Zhang, *Joule* **2022**, *6*, 444.
[45] G. Zhang, X. K. Chen, J. Xiao, P. C. Y. Chow, M. Ren, G. Kupgan, X. Jiao, C. C. S. Chan, X. Du, R. Xia, Z. Chen, J. Yuan, Y. Zhang, S. Zhang, Y. Liu, Y. Zou, H. Yan, K. S. Wong, V. Coropceanu, N. Li, C. J. Brabec, J. L. Bredas, H. L. Yip, Y. Cao, *Nat. Commun.* **2020**, *11*, 3943.
[46] E. Sağlamkaya, A. Musiienko, M. S. Shadabroo, B. Sun, S. Chandrabose, O. Shargaieva, G. M. Lo Gerfo, N. F. van Hulst, S. Shoaee, *Mater. Horiz.* **2023**, *10*, 1825.
[47] D. B. Riley, O. J. Sandberg, W. Li, P. Meredith, A. Armin, *Phys. Rev. Appl.* **2022**, *17*, 024076.
[48] Y. Firdaus, V. M. Le Corre, S. Karuthedath, W. Liu, A. Markina, W. Huang, S. Chattopadhyay, M. M. Nahid, M. I. Nugraha, Y. Lin, A. Seitkhan, A. Basu, W. Zhang, I. McCulloch, H. Ade, J. Labram, F. Laquai, D. Andrienko, L. J. A. Koster, T. D. Anthopoulos, *Nat. Commun.* **2020**, *11*, 5220.
[49] J. Luke, E. J. Yang, C. Labanti, S. Y. Park, J. S. Kim, *Nat. Rev. Mater.* **2023**, *8*, 839.
[50] Y. Qiu, J. Shi, R. Peng, X. Li, Z. Ge, *Adv. Opt. Mater.* **2024**, *12*, 2302548.
[51] S. Lai, Y. Cui, Z. Chen, X. Xia, P. Zhu, S. Shan, L. Hu, X. Lu, H. Zhu, X. Liao, Y. Chen, *Adv. Mater.* **2024**, *36*, 2313105.
[52] C. He, Y. Pan, G. Lu, B. Wu, X. Xia, C. Ma, Z. Chen, H. Zhu, X. Lu, W. Ma, L. Zuo, H. Chen, *Adv. Mater.* **2022**, *34*, 2203379.
[53] W. Wu, Y. Luo, T. A. Dela Peña, J. Yao, M. Qammar, M. Li, H. Yan, J. Wu, R. Ma, G. Li, *Adv. Energy Mater.* **2024**, *14*, 2400354.
[54] Y. Liu, F. Liu, H.-W. Wang, D. Nordlund, Z. Sun, S. Ferdous, T. P. Russell, *ACS Appl. Mater. Interfaces* **2015**, *7*, 653.
[55] D. Li, C. Guo, X. Zhang, B. Du, C. Yu, P. Wang, S. Cheng, L. Wang, J. Cai, H. Wang, D. Liu, H. Yao, Y. Sun, J. Hou, T. Wang, *Sci. China Chem.* **2022**, *65*, 373.
[56] C. Guo, Y. Fu, D. Li, L. Wang, B. Zhou, C. Chen, J. Zhou, Y. Sun, Z. Gan, D. Liu, W. Li, T. Wang, *Adv. Mater.* **2023**, *35*, 2304921.
[57] Q. He, W. Sheng, M. Zhang, G. Xu, P. Zhu, H. Zhang, Z. Yao, F. Gao, F. Liu, X. Liao, Y. Chen, *Adv. Energy Mater.* **2021**, *11*, 2003390.
[58] Z. Gan, L. Wang, J. Cai, C. Guo, C. Chen, D. Li, Y. Fu, B. Zhou, Y. Sun, C. Liu, J. Zhou, D. Liu, W. Li, T. Wang, *Nat. Commun.* **2023**, *14*, 6297.
[59] D. Li, N. Deng, Y. Fu, C. Guo, B. Zhou, L. Wang, J. Zhou, D. Liu, W. Li, K. Wang, Y. Sun, T. Wang, *Adv. Mater.* **2023**, *35*, 2208211.
[60] M. Xie, L. Zhu, J. Zhang, T. Wang, Y. Li, W. Zhang, Z. Fu, G. Zhao, X. Hao, Y. Lin, H. Zhou, Z. Wei, K. Lu, *Adv. Energy Mater.* **2024**, *14*, 2400214.
[61] H. Mao, J. Zhang, X. Cen, J. Zhang, L. Wen, J. Xue, D. Luo, L. Zhang, Z. Qin, W. Ma, L. Tan, Y. Chen, *Energy Environ. Sci.* **2024**, *17*, 6799.
[62] W. Li, M. Chen, J. Cai, E. L. K. Spooner, H. Zhang, R. S. Gurney, D. Liu, Z. Xiao, D. G. Lidzey, L. Ding, T. Wang, *Joule* **2019**, *3*, 819.
[63] D. Li, C. Guo, X. Zhang, B. Du, P. Wang, S. Cheng, J. Cai, H. Wang, D. Liu, H. Yao, J. Hou, T. Wang, *Aggregate* **2022**, *3*, 104.
[64] B. Du, Y. Ma, C. Guo, J. Cai, D. Li, S. Cheng, D. Liu, Q. Zheng, T. Wang, *Adv. Funct. Mater.* **2021**, *31*, 2105794.
[65] Y. Zheng, R. Sun, M. Zhang, Z. Chen, Z. Peng, Q. Wu, X. Yuan, Y. Yu, T. Wang, Y. Wu, X. Hao, G. Lu, H. Ade, J. Min, *Adv. Energy Mater.* **2021**, *11*, 2102135.
[66] Y. Xie, C. Zhou, X. Ma, S. Y. Jeong, H. Y. Woo, F. Huang, Y. Yang, H. Yu, J. Li, F. Zhang, K. Wang, X. Zhu, *Adv. Energy Mater.* **2024**, *14*, 2400013.
[67] X. Chen, Y. Li, W. Jing, T. Zhou, X. Xu, Y. Duan, L. Yu, R. Li, Q. Peng, *Angew. Chem., Int. Ed.* **2024**, *63*, 202402831.
[68] Q. Li, X. Liao, Y. Sun, Y. Xu, S. Liu, L. M. Wang, Z. Cao, X. Zhan, T. Zhu, B. Xiao, Y. Cai, F. Huang, *Small* **2024**, *20*, 2308165.
[69] L. Zhan, S. Li, X. Xia, Y. Li, X. Lu, L. Zuo, M. Shi, H. Chen, *Adv. Mater.* **2021**, *33*, 2007231.
[70] K. Jiang, J. Zhang, Z. Peng, F. Lin, S. Wu, Z. Li, Y. Chen, H. Yan, H. Ade, Z. Zhu, A. K. Y. Jen, *Nat. Commun.* **2021**, *12*, 468.
[71] Y. Wang, H. Yu, X. Wu, D. Zhao, S. Zhang, X. Zou, B. Li, D. Gao, Z. Li, X. Xia, X. Chen, X. Lu, H. Yan, C. Chueh, A. K. Y. Jen, Z. Zhu, *Adv. Energy Mater.* **2022**, *12*, 2202729.
[72] L. Wang, C. Chen, Y. Fu, C. Guo, D. Li, J. Cheng, W. Sun, Z. Gan, Y. Sun, B. Zhou, C. Liu, D. Liu, W. Li, T. Wang, *Nat. Energy* **2024**, *9*, 208.
[73] Y. Cai, Q. Li, G. Lu, H. S. Ryu, Y. Li, H. Jin, Z. Chen, Z. Tang, G. Lu, X. Hao, H. Y. Woo, C. Zhang, Y. Sun, *Nat. Commun.* **2022**, *13*, 2369.
[74] K. Jiang, J. Zhang, C. Zhong, F. R. Lin, F. Qi, Q. Li, Z. Peng, W. Kaminsky, S. H. Jang, J. Yu, X. Deng, H. Hu, D. Shen, F. Gao, H. Ade, M. Xiao, C. Zhang, A. K. Y. Jen, *Nat. Energy* **2022**, *7*, 1076.
[75] Y. Zhang, K. Liu, J. Huang, X. Xia, J. Cao, G. Zhao, P. W. K. Fong, Y. Zhu, F. Yan, Y. Yang, X. Lu, G. Li, *Nat. Commun.* **2021**, *12*, 4815.
[76] H. Zhang, Y. Liu, G. Ran, H. Li, W. Zhang, P. Cheng, Z. Bo, *Adv. Mater.* **2024**, *36*, 2400521.
[77] Q. Chen, H. Huang, G. Ran, C. Zhang, D. Hu, X. Xu, W. Zhang, C. Yang, Y. Wu, Z. Bo, *ACS Appl. Mater. Interfaces* **2023**, *15*, 46138.
[78] Q. Chen, H. Huang, D. Hu, C. Zhang, X. Xu, H. Lu, Y. Wu, C. Yang, Z. Bo, *Adv. Mater.* **2023**, *35*, 2211372.
[79] Q. Chen, Z. Bian, Y. Yang, X. Cui, C. Jeffreys, X. Xu, W. Li, Y. Liu, M. Heeney, Z. Bo, *Angew. Chem., Int. Ed.* **2024**, *63*, 202405949.

[80] J. Zhang, M. H. Futscher, V. Lami, F. U. Kosasih, C. Cho, Q. Gu, A. Sadhanala, A. J. Pearson, B. Kan, G. Divitini, X. Wan, D. Credgington, N. C. Greenham, Y. Chen, C. Ducati, B. Ehrler, Y. Vaynzof, R. H. Friend, A. A. Bakulin, *Adv. Energy Mater.* **2019**, *9*, 1902145.
[81] R. Sun, Q. Wu, J. Guo, T. Wang, Y. Wu, B. Qiu, Z. Luo, W. Yang, Z. Hu, J. Guo, M. Shi, C. Yang, F. Huang, Y. Li, J. Min, *Joule* **2020**, *4*, 407.
[82] Z. Wang, Y. Hu, T. Xiao, Y. Zhu, X. Chen, L. Bu, Y. Zhang, Z. Wei, B. Bin Xu, G. Lu, *Adv. Opt. Mater.* **2019**, *7*, 1900152.
[83] T. H. Lee, S. Y. Park, W. W. Park, X. Du, J. H. Son, N. Li, O. H. Kwon, H. Y. Woo, C. J. Brabec, J. Y. Kim, *ACS Energy Lett.* **2020**, *5*, 1628.
[84] R. Sun, J. Guo, C. Sun, T. Wang, Z. Luo, Z. Zhang, X. Jiao, W. Tang, C. Yang, Y. Li, J. Min, *Energy Environ. Sci.* **2019**, *12*, 384.
[85] R. Sun, J. Guo, Q. Wu, Z. Zhang, W. Yang, J. Guo, M. Shi, Y. Zhang, S. Kahmann, L. Ye, X. Jiao, M. A. Loi, Q. Shen, H. Ade, W. Tang, C. J. Brabec, J. Min, *Energy Environ. Sci.* **2019**, *12*, 3118.
[86] A. Karki, J. Vollbrecht, A. L. Dixon, N. Schopp, M. Schrock, G. N. M. Reddy, T. Nguyen, *Adv. Mater.* **2019**, *31*, 1903868.
[87] A. Moliton, J. M. Nunzi, *Polym. Int.* **2006**, *55*, 583.
[88] B. Qi, J. Wang, *Phys. Chem. Chem. Phys.* **2013**, *15*, 8972.
[89] W. Shockley, H. J. Queisser, *J. Appl. Phys.* **1961**, *32*, 510.
[90] F. Wei, L. Liu, L. Liu, G. Li, in *2012 IEEE 38th Photovolt. Spec. Conf. PART 2*, IEEE, New York **2012**, 1.
[91] N. R. Tummala, S. A. Elroby, S. G. Aziz, C. Risko, V. Coropceanu, J. L. Brédas, *J. Phys. Chem. C* **2016**, *120*, 17242.
[92] J. C. Blakesley, D. Neher, *Phys. Rev. B* **2011**, *84*, 075210.
[93] A. M. Kay, M. E. Fitzsimons, G. Burwell, P. Meredith, A. Armin, O. J. Sandberg, *Sol. RRL* **2023**, *7*, 2300277.
[94] P. Hartnagel, S. Ravishankar, B. Klingebiel, O. Thimm, T. Kirchartz, *Adv. Energy Mater.* **2023**, *13*, 2300329.
[95] A. D. Scaccabarozzi, A. Basu, F. Aniés, J. Liu, O. Z Arteaga, R. Warren, Y. Firdaus, M. I. Nugraha, Y. Lin, M. Campoy Quiles, N. Koch, C. Müller, L. Tsetseris, M. Heeney, T. D. Anthopoulos, *Chem. Rev.* **2022**, *122*, 4420.
[96] P. I. Djurovich, E. I. Mayo, S. R. Forrest, M. E. Thompson, *Org. Electron.* **2009**, *10*, 515.
[97] S. Difley, T. Van Voorhis, *J. Chem. Theory Comput.* **2011**, *7*, 594.
[98] J. Ku, Y. Lansac, Y. H. Jang, *J. Phys. Chem. C* **2011**, *115*, 21508.
[99] K. M. Katubi, A. M. S. Pembere, M. Y. Mehboob, M. S. Al Buriahi, *Int. J. Quantum Chem.* **2022**, *122*, 26998.
[100] M. Haroon, A. A. Al-Saadi, M. R. S. A. Janjua, *J. Phys. Org. Chem.* **2022**, *35*, 4314.
[101] J. Bertrandie, J. Han, C. S. P. De Castro, E. Yengel, J. Gorenflot, T. Anthopoulos, F. Laquai, A. Sharma, D. Baran, J. Bertrandie, J. Han, C. S. P. De Castro, E. Yengel, J. Gorenflot, T. Anthopoulos, F. Laquai, A. Sharma, D. Baran, *Adv. Mater.* **2022**, *34*, 2202575.
[102] R. E. M Willems, C. H. L Weijtens, X. de Vries, R. Coehoorn, R. A. J Janssen, R. E. M Willems, C. H. L Weijtens, X. de Vries, R. Coehoorn, R. A. J Janssen, *Adv. Energy Mater.* **2019**, *9*, 1803677.
[103] B. Lei, Y. Yao, A. Kumar, Y. Yang, V. Ozolins, *J. Appl. Phys.* **2008**, *104*, 24504.
[104] F. Yang, S. R. Forrest, *ACS Nano* **2008**, *2*, 1022.
[105] H. Bässler, *Phys. status solidi* **1993**, *175*, 15.
[106] P. K. Watkins, A. B. Walker, G. L. B. Verschoor, *Nano Lett.* **2005**, *5*, 1814.
[107] C. Groves, R. G. E. Kimber, A. B. Walker, *J. Chem. Phys.* **2010**, *133*, 42.
[108] K. Zojer, *Adv. Opt. Mater.* **2021**, *9*, 2100219.
[109] D. Balzer, T. J. A. M. Smolders, D. Blyth, S. N. Hood, I. Kassal, *Chem. Sci.* **2021**, *12*, 2276.
[110] K. Masuda, Y. Ikeda, M. Ogawa, H. Benten, H. Ohkita, S. Ito, *ACS Appl. Mater. Interfaces* **2010**, *2*, 236.
[111] X. Li, X. Du, J. Zhao, H. Lin, C. Zheng, S. Tao, *Sol. RRL* **2021**, *5*, 2000592.
[112] T. Upreti, C. Tormann, M. Kemerink, *J. Phys. Chem. Lett.* **2022**, *13*, 6514.
[113] R. Sun, T. Wang, X. Yang, Y. Wu, Y. Wang, Q. Wu, M. Zhang, C. J. Brabec, Y. Li, J. Min, *Nat. Energy* **2022**, *7*, 1087.
[114] P. Weitz, V. M. Le Corre, X. Du, K. Forberich, C. Deibel, C. J. Brabec, T. Heumüller, *Adv. Energy Mater.* **2023**, *13*, 2202564.
[115] T. Kumari, I. Vyalih, M. Á. León Luna, H. Ahmed, M. Ahmad, R. Atajanov, E. Jayaraman, S. Manikandan, B. Paci, A. Di Carlo, J. W. Andreasen, V. Turkovic, M. Madsen, *Cell Reports Phys. Sci.* **2024**, *5*, 102027.
[116] H. Chen, R. Zhang, X. Chen, G. Zeng, L. Kobera, S. Abbrent, B. Zhang, W. Chen, G. Xu, J. Oh, S. H. Kang, S. Chen, C. Yang, J. Brus, J. Hou, F. Gao, Y. Li, Y. Li, *Nat. Energy* **2021**, *6*, 1045.
[117] Y. Wang, H. Gao, M. Sun, C. Lin, H. Li, F. R. Lin, B. Fan, Z. Li, J. A. Zapien, A. K. Y. Jen, *Adv. Energy Mater.* **2024**, *14*, 2304449.
[118] R. Basu, F. Gumpert, J. Lohbreier, P. O. Morin, V. Vohra, Y. Liu, Y. Zhou, C. J. Brabec, H. J. Egelhaaf, A. Distler, *Joule* **2024**, *8*, 970.
[119] Q. Burlingame, M. Ball, Y. L. Loo, *Nat. Energy* **2020**, *5*, 947.
[120] H. Chen, W. Sun, R. Zhang, Y. Huang, B. Zhang, G. Zeng, J. Ding, W. Chen, F. Gao, Y. Li, Y. Li, *Adv. Mater.* **2024**, *36*, 2402350.
[121] C. Zhao, R. Ma, Y. Hou, L. Zhu, X. Zou, W. Xiong, H. Hu, L. Wang, H. Yu, Y. Wang, G. Zhang, J. Yi, L. Chen, D. Wu, T. Yang, G. Li, M. Qiu, H. Yan, S. Li, G. Zhang, *Adv. Energy Mater.* **2023**, *13*, 2300904.
[122] X. Chen, R. Huang, Y. Han, W. Zha, J. Fang, J. Lin, Q. Luo, Z. Chen, C. Q. Ma, *Adv. Energy Mater.* **2022**, *12*, 2200044.
[123] S. Luo, C. Li, J. Zhang, X. Zou, H. Zhao, K. Ding, H. Huang, J. Song, J. Yi, H. Yu, K. S. Wong, G. Zhang, H. Ade, W. Ma, H. Hu, Y. Sun, H. Yan, *Nat. Commun.* **2023**, *14*, 6964.
[124] L. Ye, Y. Xiong, Z. Chen, Q. Zhang, Z. Fei, R. Henry, M. Heeney, B. T. O'Connor, W. You, H. Ade, *Adv. Mater.* **2019**, *31*, 1808153.
[125] C. Xie, X. Zeng, C. Li, X. Sun, S. Liang, H. Huang, B. Deng, X. Wen, G. Zhang, P. You, C. Yang, Y. Han, S. Li, G. Lu, H. Hu, N. Li, Y. Chen, *Energy Environ. Sci.* **2024**, *17*, 2441.
[126] P. Li, A. Hoff, A. Gasonoo, M. R. Niazi, M. Nazari, G. C. Welch, *Adv. Mater. Interfaces* **2023**, *10*, 2202156.
[127] J. Zhang, H. Mao, K. Zhou, L. Zhang, D. Luo, P. Wang, L. Ye, Y. Chen, *Adv. Mater.* **2024**, *36*, 2309379.
[128] S. Liu, H. Li, X. Wu, D. Chen, L. Zhang, X. Meng, L. Tan, X. Hu, Y. Chen, *Adv. Mater.* **2022**, *34*, 2201604.
[129] W. Song, J. Ge, L. Xie, Z. Chen, Q. Ye, D. Sun, J. Shi, X. Tong, X. Zhang, Z. Ge, *Nano Energy* **2023**, *116*, 108805.
[130] M. Charles, B. Edwards, E. Ravishankar, J. Calero, R. Henry, J. Rech, C. Saravitz, W. You, H. Ade, B. O'Connor, H. Sederoff, *Front. Plant Sci.* **2023**, *14*, 1087707.
[131] A. M. Kay, D. B. Riley, O. J. Sandberg, G. Burwell, P. Meredith, A. Armin, *Sol. RRL* **2024**, *8*, 2400456.
[132] M. H. Riaz, H. Imran, H. Alam, M. A. Alam, N. Z. Butt, *IEEE J. Photovoltaics* **2022**, *12*, 572.
[133] G. K. Grandhi, G. Koutsourakis, J. C. Blakesley, F. De Rossi, F. Brunetti, S. Öz, A. Sinicropi, M. L. Parisi, T. M. Brown, M. J. Carnie, R. L. Z. Hoye, P. Vivo, *Nat. Rev. Clean Technol.* **2025**, *1*, 132.
[134] V. Pecunia, L. G. Occhipinti, R. L. Z. Hoye, *Adv. Energy Mater.* **2021**, *11*, 2100698.
[135] M. Jahandar, S. Kim, D. C. Lim, *ChemSusChem* **2021**, *14*, 3449.
[136] B. Zhang, J. C. Bonner, L. N. S. Murthy, T. A. Nguyen, F. Y. Cao, Y. J. Cheng, B. H. Hamadani, J. W. P. Hsu, *Org. Electron.* **2022**, *104*, 106477.
[137] K. Seunarine, Z. Haymoor, M. Spence, G. Burwell, A. Kay, P. Meredith, A. Armin, M. Carnie, *J. Phys. Energy* **2024**, *6*, 015018.
[138] D. Lübke, P. Hartnagel, J. Angona, T. Kirchartz, *Adv. Energy Mater.* **2021**, *11*, 2101474.
[139] G. Burwell, O. J. Sandberg, W. Li, P. Meredith, M. Carnie, A. Armin, *Sol. RRL* **2022**, *6*, 2200315.